the XUV one-photon process. Because of the frequency relation between the odd-harmonic XUV comb and the fundamental MIR laser, the resonant EWP upshifted by absorption of a MIR photon, $A_{R+1}(\tau, E + \hbar\omega_0) \propto A_R(E) \exp(i\omega_0\tau)$, and the reference EWP downshifted by stimulated emission of a MIR photon, $A_{NR-1}(\tau, E + \hbar\omega_0) \propto A_{NR}(E + 2\hbar\omega_0) \exp(-i\omega_0\tau)$, coherently add up in the single sideband (SB_{64}) that lies between the lines associated with H_{63} and H_{65}. Similarly, the resonant EWP downshifted by emission of a MIR photon interferes in sideband SB_{62} with the EWP upshifted by absorption of a MIR photon from H_{61}. We designate E the photoelectron energy in the resonant EWP, and $\overline{E} = E \pm \hbar\omega_0$ the photoelectron energy of the resonant EWP replicas in SB_{64} and SB_{62}, respectively.

The spectrum of these sidebands is thus modulated by the interference between the resonant and nonresonant replicas, depending on the XUV-MIR delay τ (*25*). For SB_{64}, the spectrum is given by

$$\begin{aligned} S_{64}(\tau, \overline{E}) &= |A_{R+1}(\tau, \overline{E}) + A_{NR-1}(\tau, \overline{E})|^2 \\ &= |A_{R+1}(\overline{E})|^2 + |A_{NR-1}(\overline{E})|^2 + \\ &\quad 2|A_{R+1}(\overline{E})||A_{NR-1}(\overline{E})| \\ &\quad \times \cos[2\omega_0\tau + \Delta\varphi_{64}(\overline{E}) + \Delta\eta_{scat}(\overline{E})] \end{aligned} \quad (1)$$

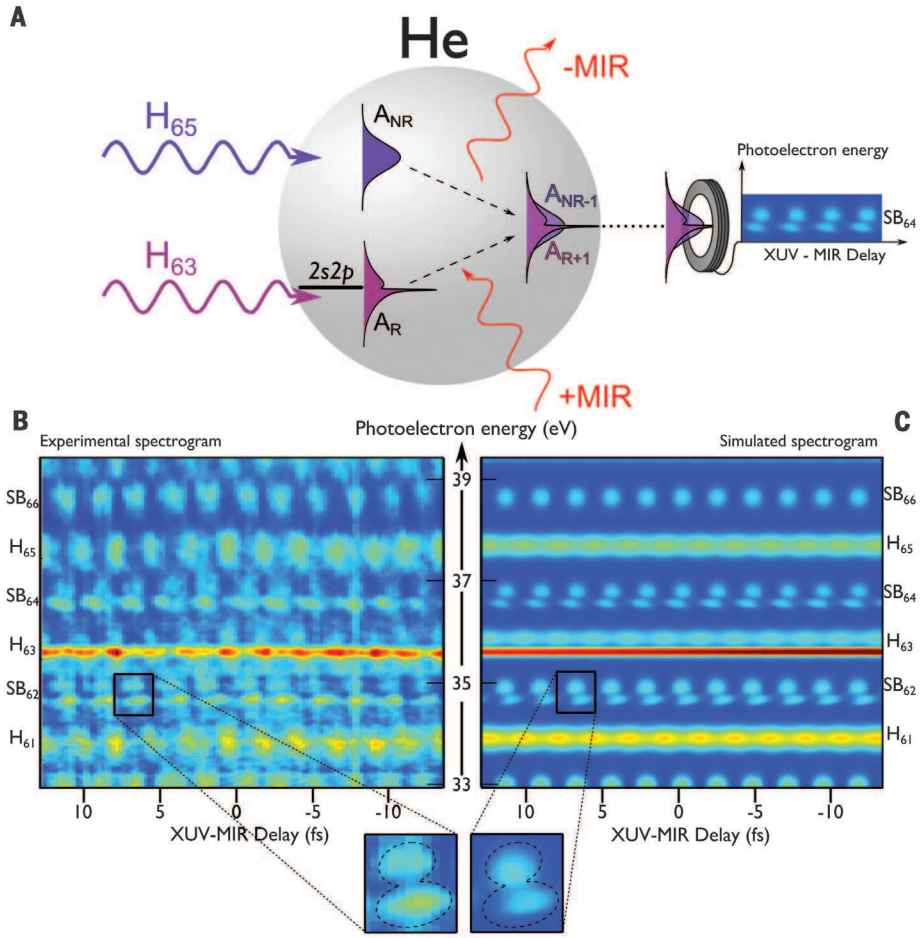

Fig. 1. Principle and resulting spectrogram of spectrally resolved attosecond electron interferometry for the complete characterization of resonant EWPs. (**A**) Principle of the electron interferometry technique. Resonant A_R and reference nonresonant A_{NR} EWPs are produced by successive coherent harmonics. Replicas of these EWPs are created at the same final energy by two-photon transitions induced by a weak fundamental MIR field, where the atom absorbs a MIR photon, leading to the A_{R+1} EWP, or emits a MIR photon, leading to the A_{NR-1} EWP. The spectrally resolved interferences are measured in a time-of-flight electron spectrometer as a function of the XUV-MIR delay τ, controlled with interferometric accuracy; these interferences provide access to the spectral phase of the resonant A_R EWP. (**B** and **C**) Experimental spectrogram (B) and theoretical spectrogram (C) in the 33- to 39-eV region for a 1295-nm OPA wavelength (*25*). H_{63} overlaps the 2s2p resonance of helium located 60.15 eV above the ground state (E_R = 35.55 eV). Single-photon ionization by the odd harmonic orders results in main lines spaced by twice the MIR photon energy, $2\hbar\omega_0$ = 1.92 eV. Between these lines appear sidebands corresponding to two-photon ionization. The oscillations of the two sidebands on both sides of the resonant H_{63} (i.e., SB_{62} and SB_{64}) encode the spectral phase of the resonant EWP. A close-up of one SB_{62} beating shows the structured shape of this resonant EWP and the dephasing of the oscillations of the different spectral components.

where the two contributions to the replicas' relative phase are (i) $2\omega_0\tau$, the phase introduced by the absorption or simulated emission of the MIR photon, and (ii) the relative phase between the initial one-photon EWPs. The latter is split into $\Delta\varphi_{64}(\overline{E}) = \varphi_{65}(\overline{E} + \hbar\omega_0) - \varphi_{63}(\overline{E} - \hbar\omega_0)$, the phase difference between the two ionizing harmonics, and $\Delta\eta_{scat}(\overline{E}) = \eta_{scat}(\overline{E} + \hbar\omega_0) - \eta_{scat}(\overline{E} - \hbar\omega_0)$, the difference between the nonresonant and resonant scattering phases of the two intermediate states. In our conditions, the variations over the sideband width of both $\Delta\varphi_{64}(\overline{E})$ and $\eta_{scat}(\overline{E} + \hbar\omega_0)$ are negligible in comparison with that of the resonant scattering phase $\eta_{scat}(\overline{E} - \hbar\omega_0)$ (*25*). The latter contains information about the scattering of the photoelectron by the remaining core, including strongly correlated scattering by the other electron close to the resonance. This phase is the measurable quantity addressed by our study.

Using a high-resolution (~1.9%) magnetic-bottle spectrometer with a length of 2 m, we have access to the photoelectron spectrogram—electron yield as a function of energy E and delay τ—spectrally resolved within the harmonics and sideband widths (Fig. 1B). As a result of its large bandwidth, H_{63} produces a photoelectron spectrum exhibiting a double structure with a Fano-type resonant peak and a smoother peak. This shape is replicated on each of the closest resonant sidebands (SB_{62} and SB_{64}). Strikingly, the components of the double structure oscillate with different phases when τ is varied, in both SB_{62} and SB_{64}.

These phase variations are further evidenced by a spectrally resolved analysis: For each sampled energy within the sideband width, we perform a Fourier transform of $S_{63\pm1}(\tau, E + \hbar\omega_0)$ with respect to τ to extract the amplitude and phase of the component oscillating at $2\omega_0$ (see Eq. 1 and Fig. 2). The SB_{62} phase shows a strong increase of ~1 rad within the resonant peak, followed by a sudden drop at the amplitude minimum ($\overline{E}$ ~ 34.75 eV), and a rather flat behavior under the smooth peak. The SB_{64} phase has a very similar shape and magnitude but with an opposite sign due to opposite configuration of the resonant and reference EWPs in the interferometer. This correspondence confirms the direct imprint of the intermediate resonance on the neighboring sidebands.

The $2\omega_0$ component of the resonant sidebands thus provides a good measure of the $|A_R(E)| \exp[i\eta_{scat}(E)]$ EWP that would result from one-photon Fourier-limited excitation. This allows a detailed study of the temporal characteristics of resonant photoemission, in particular of the electron flux into the continuum, through the direct reconstruction of this EWP in the time domain:

$$\tilde{A}_R(t) = \frac{1}{2\pi}\int_{-\infty}^{+\infty} |A_R(E)| \exp[i\eta_{scat}(E)] \exp\left(\frac{-iEt}{\hbar}\right) dE \quad (2)$$

The temporal profile obtained from SB_{64} is shown in Fig. 3A. It presents a strong peak at the